Addressing SDR Impairments for Wideband Channel Characterization using Multiband Splicing

Sigrid Dimce, Anatolij Zubow, and Falko Dressler
School of Electrical Engineering and Computer Science, TU Berlin, Germany
{dimce, zubow, dressler}@ccs-labs.org

***Abstract*—Multiband splicing is a promising technique that enables wideband channel characterization using narrow-band devices. Instead of relying on high sampling rate, it leverages frequency hopping measurements across multiple narrow-bands to reconstruct a high-resolution channel impulse response (CIR). This approach is particularly appealing in the context of fragmented spectrum, especially in license-free bands, and benefits from the inherent advantages of narrow-band devices, such as lower cost and power consumption. However, a key technical challenge lies in correcting the phase distortions introduced by switching center frequencies, which is an essential step before accurate data concatenation. In this work, we investigate hardware impairments by implementing multiband splicing on software-defined radios, specifically USRP X410. We focus on analyzing the phase distortions encountered in overlapping frequency channels. Based on this analysis, we adapt targeted compensation methods from the literature, to mitigate these distortions and enable multiband splicing despite such hardware impairments. Our results show that the splicing-estimated channel impulse response (CIR) closely matches the reference wideband CIR, demonstrating the successful reconstruction of the channel.**

I. Introduction

Integrating sensing capabilities into existing communication systems is a key goal for future 6G networks [1]. This is particularly relevant for widely deployed IEEE 802.11 (Wi-Fi) systems, which, promoted by the ability to obtain channel state information (CSI), have enabled a broad range of sensing-based applications such as ranging [2], localization [3], [4], and human or object detection [5]–[7]. However, a major limitation for Wi-Fi sensing is the restricted supported bandwidth. Even with the 802.11be standard, the maximum supported bandwidth is limited to 320 MHz, which often fails to provide the time resolution required for many sensing tasks [1].

The time resolution of the power delay profile (PDP) derived from CSI is inversely proportional to the channel bandwidth. Fine time resolution is essential for distinguishing closely spaced multipath components (MPCs) and capturing their variations, which is critical for detecting motion and small-scale environmental changes [8]. Thus, to enhance the sensing capabilities of narrow-band devices such as Wi-Fi, multiband splicing has been proposed [9].

In multiband splicing, a device performs multiple narrow-band measurements across multiple frequency bands and fuses the resulting data to reconstruct the corresponding wideband channel [10]; ideally obtaining the same results as generated by a single wideband measurement. Nonetheless, prior studies have shown that the frequency band aperture (i.e., the separation between the center frequencies of two consecutive bands) should remain within 20% of the carrier frequency to avoid significant frequency-dependent effects [11]. Numerous works have proposed algorithms that perform splicing over consecutive [8], [12] or non-consecutive bands [6], [7]. A key practical advantage of multiband splicing is its ability to cope with spectrum fragmentation, a common challenge in shared and congested unlicensed frequency bands. By enabling narrow-band measurements only in available parts of the spectrum, splicing offers a flexible and adaptive solution [10]. Another practical consideration is related to the signal-to-noise ration (SNR): wideband measurements inherently suffer from higher noise power, and when operating at the maximum transmit power, increasing the signal bandwidth reduces the power spectral density by up to 3 dB when doubling the bandwidth—further degrading the effective SNR.

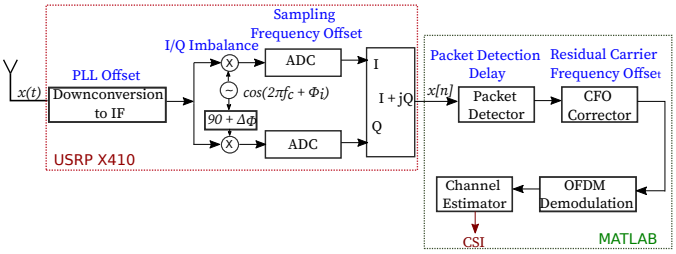

Figure 1. Illustration of the receiver chain from signal capture to channel estimation, including sources for phase distortions.

Despite these advantages, multiband splicing faces two key challenges. First, the measurements across different center frequencies must be performed within the channel coherence time, a requirement that becomes particularly difficult to meet in mobile scenarios. Second, phase distortions introduced during the switching between center frequencies must be corrected for each narrow-band channel. These impairments must be compensated prior to splicing to ensure accurate reconstruction of the wideband channel.

In this work, we investigate the feasibility of implementing multiband splicing using software defined radio (SDR) hardware, specifically the USRP X410, already widely used in research and academia. We focus on understanding the phase offset challenges encountered when applying multiband splicing with SDR hardware and overlapping frequency channel. Our goal is to identify the underlying sources of hardware-induced phase distortions and develop targeted compensation methods to mitigate their effects.

Our key contributions can be summarized as follows:

- We conduct extensive measurements using USRP X410 SDR platform to analyze phase distortions introduced by underlying hardware when switching center frequencies.
- We identify the sources of hardware-induced phase offsets and adapt targeted correction techniques to compensate for each type of distortion.
- We use multiband splicing concatenating the phase-corrected measurements obtained across overlapping frequency bands, and validate the results.

II. Related Work

Channel frequency samples acquired across multiple bands are subject to time and phase offsets, which must be estimated and compensated before the samples can be concatenated to reconstruct a high-resolution channel impulse response (CIR). Several studies have addressed this problem [2]–[4], [6], [7].

One of the first approaches to multiband splicing by Khalilsarai et al. [13] focused solely on the magnitude of the channel frequency response samples, ignoring the phase component. Later, the same authors introduced an improved method that incorporates both magnitude and phase, recognizing the importance of phase information for accurate reconstruction [4]. This algorithm utilizes compressed sensing, specifically atomic norm denoising, to identify and remove phase distortion components within each band. Other studies adopted a more systematic approach by identifying the specific sources of error and proposing targeted compensation strategies [8], [14]. These methods operate across consecutively scanned frequency bands and were validated through experiments using real-world measurements.

More recent works have shifted the focus toward non-overlapping/non-consecutive multiband splicing. The HiSAC framework [6] tackles hardware impairments such as carrier frequency offset (CFO), timing offset, and random phase shifts by using a shared anchor path across subsystems to estimate and correct time and phase offsets, under the assumption of short-term channel stability. Li et al. [7] introduced a model-driven deep learning approach to reconstruct radar-like time of flight (ToF) and angle of arrival (AoA) spectra from sparse Wi-Fi channel measurements. Although this method does not explicitly compensate for hardware distortions, it implicitly learns to handle such effects through training on synthetic data that models them. Helwa et al. [2] propose a multiband approach for indoor distance ranging using the USRP X310. To overcome the phase and time offset issue, a two-way approach is proposed, relying on channel reciprocity.

In this work, we exhaustively explore hardware-induced distortions using the USRP X410, a high-performance SDR platform that supports fully configurable waveforms. Unlike previous studies relying on SDR hardware [2], we do not assume channel reciprocity, and have no local oscillator (LO) sharing.In this context, we propose a novel algorithm that estimates and compensates for phase offsets using real measurement data collected over overlapping frequency bands.

III. Background and Experiment Setup

State-of-the-art wireless technologies, such as Wi-Fi and 5G, are based on the orthogonal frequency division multiplexing (OFDM) waveform, so integrating sensing here, is important. In an OFDM system, the received signal on the k-th subcarrier in the frequency domain is modeled as:

$$y[k] = H[k] \cdot s[k] + z[k], \tag{1}$$

where $y[k]$ is the received symbol, $s[k]$ is the transmitted symbol, $z[k]$ represents the additive noise, and $H[k]$ denotes the channel frequency response (CFR) at subcarrier k. In single-antenna systems, the CSI is equivalent to the CFR, which characterizes the wireless channel in the frequency domain. The CFR is a complex value and captures both the magnitude and phase changes introduced by the channel. To analyze the channel in time domain, the CIR can be obtained by an inverse fast Fourier transformation (IFFT) of the estimated CFR:

$$h[n] = \text{IFFT}\{H[k]\}, \tag{2}$$

where, $h[n]$ is the CIR at delay index n. The CIR describes the arrival times and the relative strengths of MPCs, offering insights into the delay profile of the channel. The temporal resolution of the CIR, i.e., the ability to resolve two multipath components having similar delays, is inversely proportional to the signal bandwidth:

$$\Delta\tau = 1/B, \tag{3}$$

where B is the signal bandwidth, $\Delta\tau$ is the resolvable time delay between two paths. Therefore, a wider bandwidth yields finer time resolution, enabling better separation of multipath signals with same delays.

To conduct our experiments, we deployed an indoor testbed comprising the following hardware components:

- SDR: USRP X410 (National Instruments), each configured with a master clock rate of 500 MHz.
- Clock synchronization: OctoClock CDA-2990 (National Instruments), providing 10 MHz frequency reference and 1 PPS timing pulse to synchronize the SDRs.
- Host system: AMD Ryzen 9 7950X 16-Core CPU with 128 GB RAM, equipped with a 100 Gbit/s interface.

Each SDR is connected to the host machine via a 100 Gbit/s Ethernet link to ensure fast data transfer. On the software side, we utilized the MATLAB WLAN Toolbox to generate and decode IEEE 802.11be frames relying on OFDM waveform. Experiments were conducted using 20 MHz, 40 MHz, 160 MHz and 320 MHz channel bandwidth configurations. The waveforms were modulated using BPSK with a coding rate of 1/2, yielding a physical-layer data rate of 144 Mbit/s. Each waveform uses 256, 512, 2048, and 4096 subcarriers for 20 MHz, 40 MHz, 160 MHz, and 320 MHz channels, respectively, with a constant subcarrier spacing of 78.125 kHz. Each signal was upsampled to a rate of 500 MS/s for transmission on USRP. The transmitter continuously looped the waveform with a frame duration of 140 µs, while the receiver captured the incoming signal for post-processing in MATLAB. During post-processing,

packet detection was performed first, followed by decoding and channel estimation to extract channel state information. To enable channel hopping (i.e. changing the center frequency), we implemented a ZeroMQ-based PUB/SUB architecture, allowing the transmitter and receiver to communicate while changing to different center frequencies. At the receiver side, we created separate buffers in the USRP for each center frequency. After the reception phase, each buffer is saved into a distinct file, facilitating post-processing.

From each received frame, we extracted the CFR from the 802.11be EHT-LTF field using a least square (LS) estimation technique [15], computed as:

$$\hat{H}[k] = \frac{Y[k]}{X[k]}, \tag{4}$$

where $\hat{H}[k]$ is the estimated CFR for subcarrier k, $Y[k]$ denotes the received symbols, and $X[k]$ are the known transmitted reference symbols. The DC subcarrier is recovered via interpolation between the two adjacent subcarrier, and only the active subcarriers (excluding the left and right null subcarriers) are retained for subsequent processing.

Finally, we derived the CIR, representing the channel in the time domain, by applying the IFFT to the CFR.

To investigate hardware-induced distortions in the context of multiband splicing, we designed a controlled wired environment using RF splitters, combiners, and coaxial cables. The RF splitter is connected to the output port of the USRP X410 transmitter and splits the output signal into two copies, which go through different cable lengths (multipath components). On the other side, the RF combiner combines the two signals coming from the two paths, and it is connected to the input port of the USRP X410 receiver. The cable lengths are 1 m and 5 m respectively.

We used a fixed frequency hopping scheme to transmit a 160 MHz signal at three center frequencies 4 GHz, 4.08 GHz, and 4.16 GHz, resulting in overlapping bands that together span a total bandwidth of 320 MHz. Both the transmitter and receiver hop to the next center frequency every 40 ms, continuously cycling and retuning to each center frequency in sequence throughout the measurement period.

An overview of the receiver chain is illustrated in Figure 1. The incoming RF signal is first downconverted to an intermediate frequency (IF) through a two-stage heterodyne architecture in the analog front-end of the USRP X410. In each stage, the signal is mixed with a LO signal, whose frequency is controlled by a phase-locked loop (PLL). Next, the signal is downconverted to baseband and then digitized using a high-speed analog to digital converter (ADC). The resulting complex baseband samples are stored on the host PC for offline processing in MATLAB. Post-processing begins by detecting the presence of a packet in the received signal through autocorrelation. Specifically, the signal is correlated with a delayed version of itself, exploiting the periodic structure of the legacy short training field (L-STF) in the Wi-Fi preamble, which would produce peaks in case a packet is present. Once the packet boundary is identified, the signal's center frequency

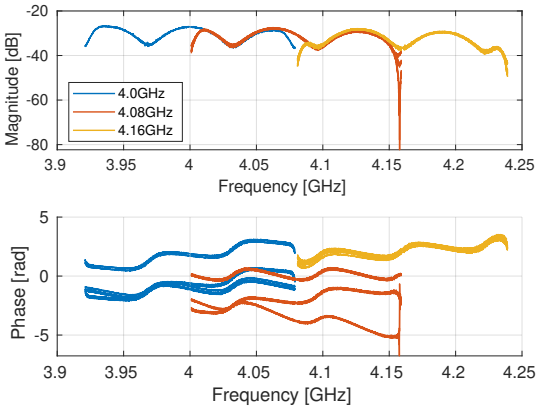

Figure 2. CFR magnitude and phase for three overlapping 160 MHz bands collected over a two path wired channel.

is calibrated by estimating and compensating for any CFO. The CFR is then estimated using a LS method, followed by equalization to mitigate the effects of multipath propagation.

In our setup, both the transmitter and receiver are connected to an OctoClock, which distributes a common timing and frequency reference. While this ensures synchronization in frequency and time, the OctoClock does not provide phase synchronization, which would require LO sharing. As a result, the measured CFR phase is subject to various impairments.

As previously discussed, the CFR is a complex value comprising both magnitude and phase. Figure 2 illustrates the raw CFR magnitude and phase collected over the cable measurements and over multiple packets and channel hoppings, i.e. center frequency retunings. While the magnitude remains relatively stable across changes to center frequency, the phase exhibits both a constant offset and a linear rotation, reinforcing the need for phase correction to enable accurate splicing across different bands.

IV. Addressing Hardware Distortions

In the following, we identify the sources of distortions and adapt solutions to mitigate each of them.

A. Nonlinear Phase Error

Theoretically, end-to-end Wi-Fi transmission can be modeled as a linear system. As discussed in [8], the phase of each subcarrier should vary linearly with its frequency, with the slope determined by the propagation path length. However, prior studies have shown that the phases of subcarriers, particularly at the edges of the frequency band, exhibit non-linear distortions [8], [14]. These distortions have been attributed to I&Q imbalance introduced during downconversion [9].

Our measurements revealed nonlinear distortions at both edges of the measured channel. To analyze this behavior, we adopted a methodology similar to that used in the literature for characterizing I&Q imbalance-induced nonlinearities. Specifically, we connected the transmitter and receiver using a single 1 m coaxial cable to isolate the channel effects like multipath propagation. Measurements are performed at the center frequency of 4 GHz across various bandwidths (20 MHz,

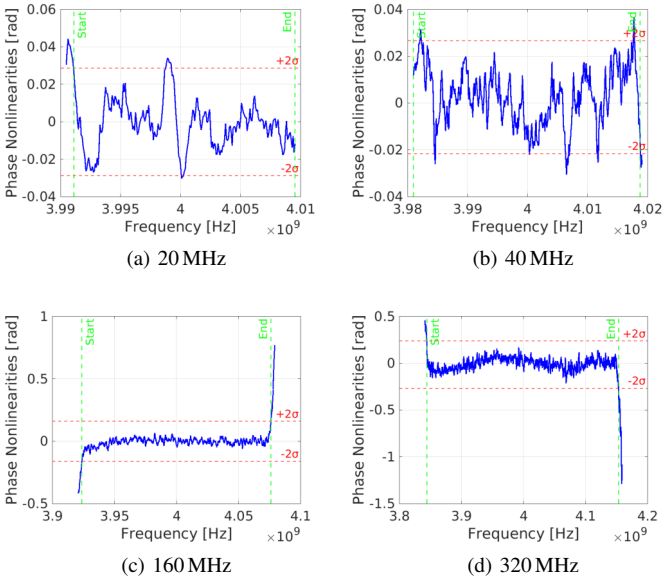

(a) 20 MHz (b) 40 MHz

(c) 160 MHz (d) 320 MHz

Figure 3. Estimated linear phase region across different channel bandwidths (single path wired channel).

40 MHz, 160 MHz, and 320 MHz), with signals upsampled to 500 MS/s. The central subcarriers exhibit linearity, which we leveraged to perform a least squares linear fitting, to estimate the slope and offset, and to predict the phase of nonlinear subcarriers, as proposed in the literature [8]. The nonlinearity is calculated as the difference between the theoretical linear phase and the measured phase, and is then used to identify the linear region for each bandwidth, as illustrated in Figure 3.

To estimate the linear region in the residual phase, we began by smoothing the data using a moving average filter with a small window size (15 samples) to suppress local fluctuations while preserving the overall trend. We then computed the mean and standard deviation of the smoothed residual, and defined a linearity threshold as $\pm 2\sigma$ around the mean. To determine the linear region for each bandwidth, we identified the range where the smoothed residual phase remained within $\pm 2\sigma$ of the mean, depicted in Figure 3 in the form of red dashed lines. Measurements were repeated at different time instances and with varying cable lengths (2 m) to assess the stability and reproducibility of the observed distortions.

We believe that the nonlinearity behavior we see at both edges of the phase is not only a result of the I&Q imbalance, but also a result of resampling and bandpass filtering. Unlike the fixed nonlinear patterns reported in studies using Wi-Fi cards [8], we observe that the nonlinearity in our setup is neither subcarrier-invariant nor time-invariant, and therefore can not be removed using calibration as proposed by [8]. Furthermore, our results indicate that the impact of these nonlinearities depends on the signal bandwidth. For narrow bandwidths such as 20 MHz and 40 MHz, the effects of resampling are minimal, allowing almost the entire bandwidth to exhibit linear behavior. In contrast, for wider bandwidths like 160 MHz and 320 MHz, the nonlinear distortions become more pronounced. This observation suggests that using narrower bandwidths – being the key concept of multiband splicing – can help mitigate these effects. However, when working with wider bandwidths, we propose discarding approximately 3% of the subcarriers at each edge of the phase spectrum prior to band concatenation, in order to reduce the influence of nonlinearities. This discarded portion is significantly smaller than what has been reported for cots Wi-Fi hardware operating at 20 MHz [8].

B. Linear Phase Error

After analyzing the effects of nonlinearities, we turned our attention to understanding the causes of the linear errors in the raw CFR data: the phase slope variations and vertical offsets. To investigate these effects, we used the setup with two coaxial cables presented in Section III, where the second path is approximately 6 dB weaker than the first. This setup differs from the previous experiment where only a single coaxial cable is used to study the non-linearities. While both the transmitter and receiver are connected to an OctoClock to maintain time and frequency synchronization, the OctoClock does not ensure phase alignment, as it would require LO sharing. Given the characteristics of the observed distortions, we divide the sources of the distortions into: phase rotation and phase offset.

1) Phase Rotation: From our collected traces, we observed that the phase slope changes within each narrow channel. This behavior can be attributed to sampling frequency offset (SFO) and packet detection delay (PDD) [8], [14]. The SFO arises from a mismatch in the sampling intervals between the transmitter and the receiver. This mismatch leads to a time shift of the received signal with respect to the transmitted signal after ADC, which manifests as a phase rotation. On the other hand, the PDD arises from a timing offset between the packet detector's estimated starting point and the real start of the packet. This time shift introduces frequency dependent phase distortions. Prior work [8] using WiFi COTS hardware shows that PDD-induced distortion follows a Gaussian distribution and can be mitigated by averaging packets within each channel.

In our data, we found that within a single center frequency (i.e., without retuning), the phase across packets varied only slightly, consistent with PDD effects. This variation also resembled a Gaussian distribution. However, after retuning, even to the same center frequency, a more significant phase slope change was observed.

To address this, we averaged the phase across all packets in each channel to extract a stable reference. Next, we adapted the phase correction strategy proposed in [8]. According to this work, the PDPs derived from different frequency bands should look the same after compensating for the slope error. The authors propose to gradually rotate the phases of a pair of frequency bands in frequency domain until the derived PDP in time domain best matches each other. We follow this approach and divided the three overlapping bands into pairs and performed an exhaustive phase rotation search for each pair by rotating the phase with an ϵ ranging from $[-0.1, 0.1]$, and computing the similarity factor of the corresponding PDPs, as shown in [8, Eq. 7]. Once the rotation error is removed, we can see that the shape of the overlapping subcarriers from the

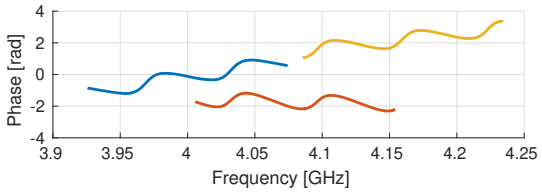

(a) Before phase correction

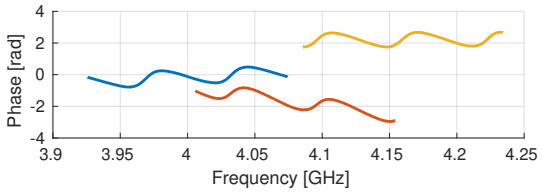

(b) After correcting for slope error

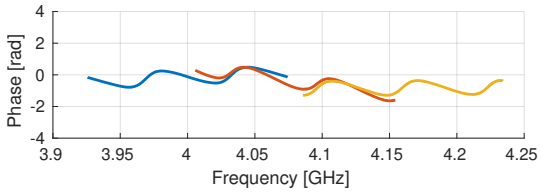

(c) After correcting for offset error

Figure 4. Phase of the independently captured overlapping 160 MHz bands.

different frequency bands now becomes similar and consistent, as depicted in Figure 4b.

For comparison, we also show the phase results before applying the rotation correction in Figure 4a. As we can see from the results, the phases over the three frequency bands are slightly rotated after the slope error correction, making the shape over the overlapping areas more similar.

2) Phase Offset: A second type of phase distortion observed in our measurements is a vertical phase offset, i.e., a constant phase delta across all subcarriers within a frequency band. Based on insights from the literature and our analysis, this offset primarily originates from two sources: the PLL and CFO. The PLL locks the frequency and phase of a local oscillator to that of a reference signal [16]. Its purpose in the radio transmitter and receivers is to generate a stable, frequency accurate local oscillator for up and down conversion. Whenever the PLL retunes to a frequency, it starts with a random initial phase offset, which is constant across the entire waveform. The CFO, on the other hand, results from a frequency mismatch between the local oscillators of the transmitter and receiver. Factors such as temperature variations and oscillator aging can cause gradual frequency drift, leading to a time-varying CFO. To mitigate this, the CFO is estimated in two stages: a coarse estimation using the L-STF, capable of estimating CFO up to 625 kHz, and a fine-grained estimation using the legacy long training field (L-LTF), which refines the estimate up to 156.25 kHz. Nevertheless, the CFO estimation and compensation are generally not-perfect, and the residual CFO will cause a phase offset. In our case, although we employ an OctoClock to distribute a common reference clock to both TX and RX, a small residual CFOs can still occur due to imperfections in frequency synthesis.

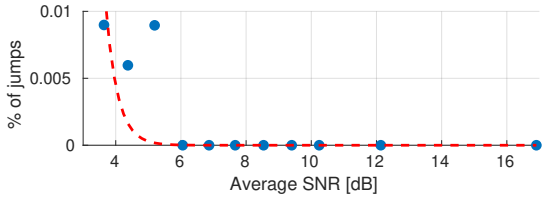

Figure 5. Percentage of received packets experiencing phase jumps as a function of SNR, along with the curve fitting the data.

Fortunately, as noted in [8], such phase offsets do not affect the derived PDP. To correct for these offsets across frequency bands, we follow the calibration method proposed in [8]: we use the phase of the first frequency band as a reference and align the phases of the remaining bands accordingly. The outcome after applying this offset compensation is shown in Figure 4c.

C. Impact of Signal-to-Noise Ratio

The impact of SNR in multipath environments is critical for sensing-based applications, particularly those that rely on accurate channel estimation. We noticed that in certain scenarios where the packets were correctly decoded, the estimated phase exhibited jumps that were multiples of π. This phase distortion disappeared when the SNR at the receiver increases. Similar phenomena were reported in [2], where deep fading was identified as a source of phase discontinuities. To study this effect systematically, we conducted repeated measurements using a single coaxial cable, eliminating multipath propagation, while gradually reducing the receiver gain.

The results are summarized in Figure 5, which shows the percentage of packets exhibiting phase jumps as a function of SNR. These results highlight an important distinction: while communication systems can tolerate lower SNR levels (e.g., 5 dB), sensing applications demand higher SNR for accurate and stable phase estimation. It is worth noting that the USRP devices used in our setup do not include an onboard automatic gain control (AGC) mechanism. However, implementing a software-based AGC on the FPGS, dynamically adjusting the receiver gain based on observed signal power, could help maintain a more consistent SNR and mitigate the observed phase instability. Finally, the issue of SNR becomes more pronounced with increasing bandwidth, as the noise power rises proportionally, i.e., 3 dB for each doubling of the bandwidth. This highlights another advantage of multiband splicing approach: by combining multiple narrow-band captures, we can achieve wideband channel reconstruction with better effective SNR compared to a single wideband measurement, improving sensing reliability in low-SNR environments.

D. Multiband Splicing using Concatenation of CFR Samples

After correcting the phase within each frequency band, in our scenario with two coaxial cables, we concatenate the CSI to construct a CIR with higher temporal resolution than what can be achieved from individual bands alone. To establish a baseline, we first consider the CIRs obtained from each individual 160 MHz measurement, as shown in Figure 6a.

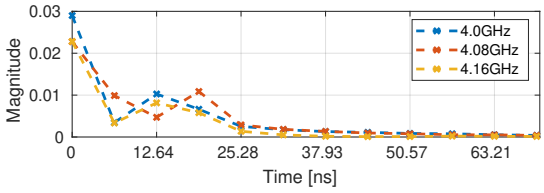

(a) CIRs from each 160 MHz measurements.

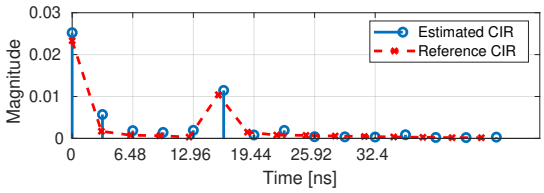

(b) Estimated CIR from splicing along with the 320 MHz CIR.

Figure 6. Estimated CIR from multiband splicing using three independent 160 MHz measurements vs. a wideband 320 MHz measurement (two path wired channel).

These measurements reflect the resolution limits of a single-band system. While the 160 MHz bandwidth is sufficient to distinguish the two propagation paths, its limited frequency span results in coarser temporal resolution.

To improve resolution, we apply a multiband splicing procedure that leverages overlapping information from three adjacent 160 MHz measurements. The concatenation follows these steps: First, we identify the overlapping frequency regions between adjacent bands. Within these overlapping areas, both the CFR magnitude and phase are averaged to ensure smooth transitions. We then merge the unique and overlapping sections, trimming the edges by 3% on both ends as previously described. This yields a new, continuous CFR, from which we compute the high-resolution CIR via IFFT. The resulting CIR is depicted in Figure 6b. To validate the accuracy of our approach, we transmit a 320 MHz signal centered at 4.08 GHz through the system and estimate the CIR at the receiver. During the measurement, we follow the same procedure used for the 160 MHz bands, retuning the receiver multiple times to the same center frequency and observing variations in the phase slope. The CFR magnitude and phase are then averaged over all packets in the trace to obtain a stable reference CIR, which is also shown in Figure 6b, alongside the spliced CIR.

As discussed earlier, our system setup includes two cables of 1 m and 5 m in length. Considering that the signal propagation speed in coaxial cables typically ranges from 66% to 85% of the speed of light in vacuum depending on the dielectric constant, the second path is expected to arrive approximately 16 ns later. This aligns well with the observed results. Most importantly, the CIR obtained through multiband splicing closely matches the reference 320 MHz CIR, demonstrating that our method can successfully reconstruct wideband channel characteristics using lower-bandwidth, frequency-hopped measurements.

V. Conclusion

In this work, we investigated issues associated with phase distortions related to multiband splicing using SDR USRP X410 hardware. Our objective was to identify the root causes of hardware-induced phase distortions and to develop targeted compensation techniques to mitigate their impact. For multi-band splicing, the system relies on overlapping frequency regions for phase alignment, due to phase slope variations occurring after retuning or after starting new measurement sessions. We proposed mitigation techniques and show that these are very effective in a controlled experimental setup. In future work, we plan to extend the experimental analysis and present results from over-the-air experiments. We aim to explore further methods for compensating hardware-induced distortions and reducing the number of required measurements for reliable phase reconstruction.

Acknowledgments

This work was supported by the Federal Ministry of Research, Technology, and Space (BMFTR, Germany) within the 6G-RIC project under grant 16KISK020K.

References

[1] H. Wymeersch, A. Pärssinen, T. E. Abrudan, A. Wolfgang, K. Haneda, M. Sarajlic, M. E. Leinonen, M. F. Keskin, H. Chen, S. Lindberg, P. Kyösti, T. Svensson, and X. Yang, "6G radio requirements to support integrated communication, localization, and sensing," in *EuCNC/6G Summit*, Grenoble, France, Jun. 2022.

[2] S. Helwa, J. P. Van Marter, S. N. Shoudha, M. Ben-Shachar, Y. Alpert, A. G. Dabak, M. Torlak, and N. Al-Dhahir, "Bridging the performance gap between two-way and one-way CSI-based 5 GHz WiFi ranging," *IEEE Access*, vol. 11, 2023.

[3] Z. Chen, G. Zhu, S. Wang, Y. Xu, J. Xiong, J. Zhao, J. Luo, and X. Wang, "M^3: Multipath assisted Wi-Fi localization with a single access point," *IEEE Transactions on Mobile Computing*, vol. 20, no. 2, 2021.

[4] M. B. Khalilsarai, B. Gross, S. Stefanatos, G. Wunder, and G. Caire, "WiFi-Based Channel Impulse Response Estimation and Localization via Multi-Band Splicing," in *IEEE GLOBECOM 2020*, Taipei, Taiwan: IEEE, Dec. 2020.

[5] A. Zubow, K. F. Petto, and F. Dressler, "One-Class Support Vector Machine for WiFi-based Device-free Indoor Presence Detection," in *European EW 2023*, Rome, Italy: IEEE, Oct. 2023.

[6] J. Pegoraro, J. O. Lacruz, M. Rossi, and J. Widmer, "HiSAC: High-Resolution Sensing with Multiband Communication Signals," arXiv, eess.SP 2407.07023, Jul. 2024.

[7] X. Li, H. Wang, J. Hu, Z. Chen, Z. Jiang, and J. Luo, "CCS-Fi: Widening Wi-Fi Sensing Bandwidth via Compressive Channel Sampling," in *IEEE INFOCOM 2025*, London, United Kingdom: IEEE, May 2025.

[8] Y. Xie, Z. Li, and M. Li, "Precise Power Delay Profiling with Commodity Wi-Fi," *IEEE Transactions on Mobile Computing*, vol. 18, no. 6, Jun. 2019.

[9] S. Dimce and F. Dressler, "Survey on Coherent Multiband Splicing Techniques for Wideband Channel Characterization," *IET Communications*, vol. 18, no. 19, Dec. 2024.

[10] S. Dimce, A. Zubow, A. Bayesteh, G. Caire, and F. Dressler, "Reconsidering Sparse Sensing Techniques for Channel Sounding using Splicing," *IEEE Transactions on Mobile Computing*, 2025.

[11] Y. Wan, Z. Hu, A. Liu, R. Du, T. X. Han, and T. Q. Quek, "OFDM-Based Multiband Sensing For ISAC: Resolution Limit, Algorithm Design, and Open Issues," *IEEE Vehicular Technology Magazine*, Jun. 2024.

[12] D. Vasisht, S. Kumar, and D. Katabi, "Decimeter-level localization with a single WiFi access point," in *USENIX NSDI 2016*, Santa Clara, CA, Mar. 2016.

[13] M. B. Khalilsarai, S. Stefanatos, G. Wunder, and G. Caire, "WiFi-based indoor localization via multi-band splicing and phase retrieval," in *IEEE SPAWC 2018*, Kalamata, Greece, Jun. 2018.

[14] Y. Zhuo, H. Zhu, H. Xue, and S. Chang, "Perceiving accurate CSI phases with commodity WiFi devices," in *IEEE INFOCOM 2017*, Atlanta, GA: IEEE, May 2017.

[15] J. Heiskala and J. Terry, *OFDM Wireless LANs: A Theoretical and Practical Guide*. Indianapolis, IN: SAMS, 2001.

[16] G.-C. Hsieh and J. C. Hung, "Phase-locked loop techniques. A survey," *IEEE Transactions on Industrial Electronics*, vol. 43, no. 6, 1996.